PASJ: Publ. Astron. Soc. Japan **45**, 43–55 (1993)

CO Observations of Arp's Interacting Galaxies

Yoshiaki SOFUE,[1] Ken-ichi WAKAMATSU,[2] Yoshiaki TANIGUCHI,[3] and Naomasa NAKAI[4]

[1] *Institute of Astronomy, The University of Tokyo, Mitaka, Tokyo 181*
[2] *Department of Physics, College of Technology, Gifu University, Gifu 501-11*
[3] *Astronomical Institute, Tôhoku University, Aoba, Sendai, Miyagi 980*
[4] *Nobeyama Radio Observatory,*Minamimaki-mura, Minamisaku-gun, Nagano 384-13*

(Received 1992 May 8; accepted 1992 July 24)

Abstract

We performed a ^{12}CO (J = 1–0) line survey involving fifty four interacting galaxies from the Arp's *Catalogue of Peculiar Galaxies*, and compared our results with various other data. The far infrared luminosities, as normalized by the CO luminosities, are much greater for interacting galaxies than for normal galaxies. From correlations with the interaction class we found that the molecular gas concentration in the central few kpc is not necessarily enhanced by interaction. However, the *efficiency* of star formation from the molecular gas increases significantly with the interaction class, which results in an apparent increase in the star-formation rate with the interaction class.

Key words: CO emission — Galaxies: interacting — Molecular gas — Starburst — Stars: formation — Interaction: tidal

1. Introduction

Starburst activity in the central regions of galaxies has been suggested to be induced by tidal interactions between galaxies. In fact, far-infrared (FIR) luminous galaxies, as observed by the IRAS, many of which are categorized as starburst galaxies, have been identified with interacting/merging galaxies (Sanders et al. 1986; Young et al. 1986, 1989a, b; Solomon and Sage 1988). It is remarkable that many starburst galaxies have been included in the *Atlas of Peculiar Galaxies* (Arp 1966), which is a collection of peculiar-morphology galaxies, and that the majority comprises interacting galaxies.

The following scenario concerning the origin of a starburst has been suggested (e.g., review by Sofue 1987): tidal interaction between galaxies results in an oval gravitational potential, which produces a bar in the innermost region of the galaxy (Noguchi 1988). Due to this bar a galactic shock wave is excited in the interstellar gas, resulting in a rapid accretion of interstellar gas toward the central region (Sørensen et al. 1976; Huntley 1978; Noguchi 1988). The accreted gas in the central region leads to the formation of massive stars. Intense UV radiation from the massive stars heats the dust in the dense molecular gas core/ring; this dust emits strong FIR emission at around 50–100 μm (Rieke 1980; Telesco 1988).

Although this scenario is atractive and seems to have been widely accepted, it was formulated based on the fact that the observed starburst galaxies, or FIR luminous galaxies, are often identified with interacting galaxies. Namely, the scenario is sample-dependent, in which only active star-forming galaxies are taken into account. On the other hand, no systematic study concerning the behavior of molecular gas, namely, the dynamics, distribution, and physical condition of the gas in general interacting galaxies, has yet been carried out.

Several questions thus arise: (a) Is a starburst or enhanced star formation a general phenomenon as a consequence of a galaxy-galaxy interaction? If so, when and in which phase of interaction does a starburst occur?

(b) Alternatively, is star formation enhanced in some particular circumstance of interaction? If so, what is this particular circumstance? More specifically, how do the star-formation rate (SFR) and efficiency (SEF) depend on the interaction class?

(c) How do the dynamics and distribution of the gaseous constituents differ from galaxy to galaxy, and how do they depend on the interaction phase and galaxy's orbit? In particular, how is the concentration of molecular gas toward the center related to the interaction phase and strength.

To answer these questions observationally, we need data concerning the gaseous component in unbiased samples of interacting galaxies. In particular, high-resolution mm-wave observations would provide information con-

* Nobeyama Radio Ovservatory (NRO) is a branch of the National Astronomical Observatory, an inter-university research institute operated by the Ministry of Education, Science and Culture.

cerning the concentration of molecular gas toward the nuclei through galaxy interactions. For this purpose we undertook a survey of the CO gas in interacting galaxies using the Nobeyama 45-m telescope. We selected sample galaxies from the *Atlas of Peculiar Galaxies* (Arp 1966), most of which are interacting systems. The present data provide information that is supplementary to observations of the global properties of interacting galaxies performed with medium-diameter telescopes (Sanders et al. 1986; Young et al. 1986, 1989a, b; Solomon and Sage 1988).

2. Observations

Observations of the ^{12}CO (J = 1–0) line emission towards Arp's interacting galaxies were made on 1990 January 17–20 and 24–28 and 1991 May 17–28. We used the 45-m telescope of the Nobeyama Radio Observatory. The 45-m antenna had a HPBW of 15″. The pointing accuracy was checked every one to two hours using SiO maser sources, and was found to be better than ±3″ through the observations. The main-beam efficiency measured by observing the planets was $\eta_{\rm mb} = 36\%$.

We used a cooled Schottky-barrier diode mixer receiver combined with a 2048-channel acousto-optical spectrometer of 250-MHz bandwidth, which covered 650 km s^{-1} at 115.27 GHz with a velocity resolution of 0.6 km s^{-1} and channel separation of 0.32 km s^{-1}. We binded every 32 or 64 channels, which yielded a final velocity resolution of 10 or 20 km s^{-1}, in order to increase the signal-to-noise ratio. The system noise temperature at the observing elevations was typically about 700 to 1000 K. The used intensity scale was the antenna temperature ($T_{\rm A}^*$) corrected for atmospheric loss.

We used a position-switching mode with the on-position being at the center of a galaxy and the two off-positions being at offsets of ±5′ from the galaxy center in the right-ascension direction. Since the total observing time per data point (usually per galaxy) was 1–2 hr, the on-source integration time was about 20–40 min. The rms noise of the resultant spectra of 10 km s^{-1} velocity resolution was about $\Delta T_{\rm A}^* \simeq 10$ mK. The reference center position of each galaxy was determined using the coordinates measuring system at the Kiso Observatory of the University of Tokyo, which gave the optical positions of nuclei with an accuracy of about ±3″ rms.

Selection of the objects to be observed was made based on the criteria given below:

(a) As many galaxies as possible of various interaction types from the Arp's catalogue could be included in order to obtain an outline concerning any dependency of the CO emission intensity on the interaction types. Some merging galaxies were included. Hence, various systems with Dahari's (1985) interaction class (IAC) ranging from 1 (weak interaction) through 6 (maximum) were included.

(b) The recession velocities are known either from optical or H I observations. Galaxies further than $\sim$ 100 Mpc ($H_0 = 75$ km s^{-1} Mpc^{-1}) were excluded, for which the sensitivity of the present observations is not sufficient.

(c) The optical center positions could be well determined either from the literature or from our measurements.

(d) Well-studied objects, such as Arp 337 (M82) and Arp 220 could be excluded.

3. Results and Discussion

We display the observed results in tables 1 and 2, and in figures 1 through 14. We discuss implications of the results on the basis of the diagrams.

3.1. *Results*

Table 1 summarizes the observed parameters; the legends to individual columns are given below. The obtained ^{12}CO (J = 1–0) line spectra are shown in figure 1. Among the fifty four observed galaxies, we did not use spectra of four galaxies (A86A, A104B, A176B, A178A), which were too noisy; these are indicated by dashes in the columns of the antenna temperature of table 1. Hence, figure 1 includes fifty spectra.

Column 1: Arp catalogue number (Arp 1966). The eastern component of each pair is denoted by A, and the western one by B.

Column 2: NGC number.

Column 3, 4: Reference center position in RA and Dec (1950). The galaxy positions were measured from the Palomar Schmidt plates using the position-measureing system at the Kiso Observatory by T. Soyano (private communication). Those not measured in this system were taken from the catalogue by Huchtmeier and Richter (1989).

Column 5: LSR velocity from Huchtmeier and Richter (1989).

Column 6: Peak antenna temperature ($T_{\rm A}^*$) of the ^{12}CO (J = 1–0) line.

Column 7: Full CO line width near the zero level.

Column 8: Integrated CO intensity ($I_{\rm CO}$) toward the center. The uppervalue of $I_{\rm CO}$was calculated from $T_{\rm A}^*$ by assuming a triangular velocity profile with an assumed width of 200 km s^{-1}, $I_{\rm CO}$= $T_{\rm A}^*$ (peak)×200/2 K km s^{-1}.

In table 2 we list the morphological types and derived quantities, such as the luminosities and their ratios. We also list the Dahari's (1985) interaction class (IAC). The legends to columns are as follows:

Column 1: Arp catalogue number.

Column 2: Morphological type. Since the galaxies are strongly disturbed, this classification is not accurate.

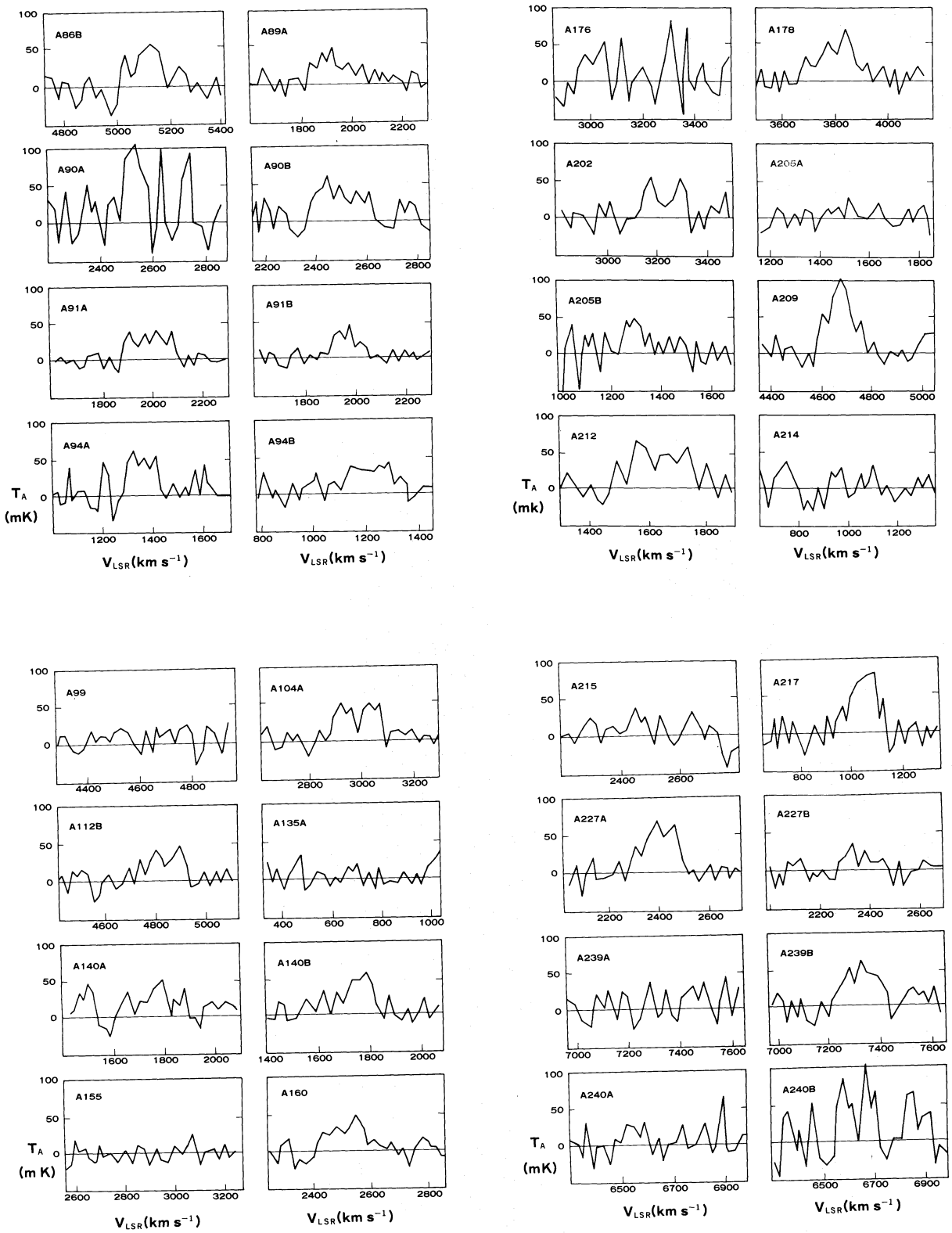

Fig. 1. CO line profiles for the observed galaxies.

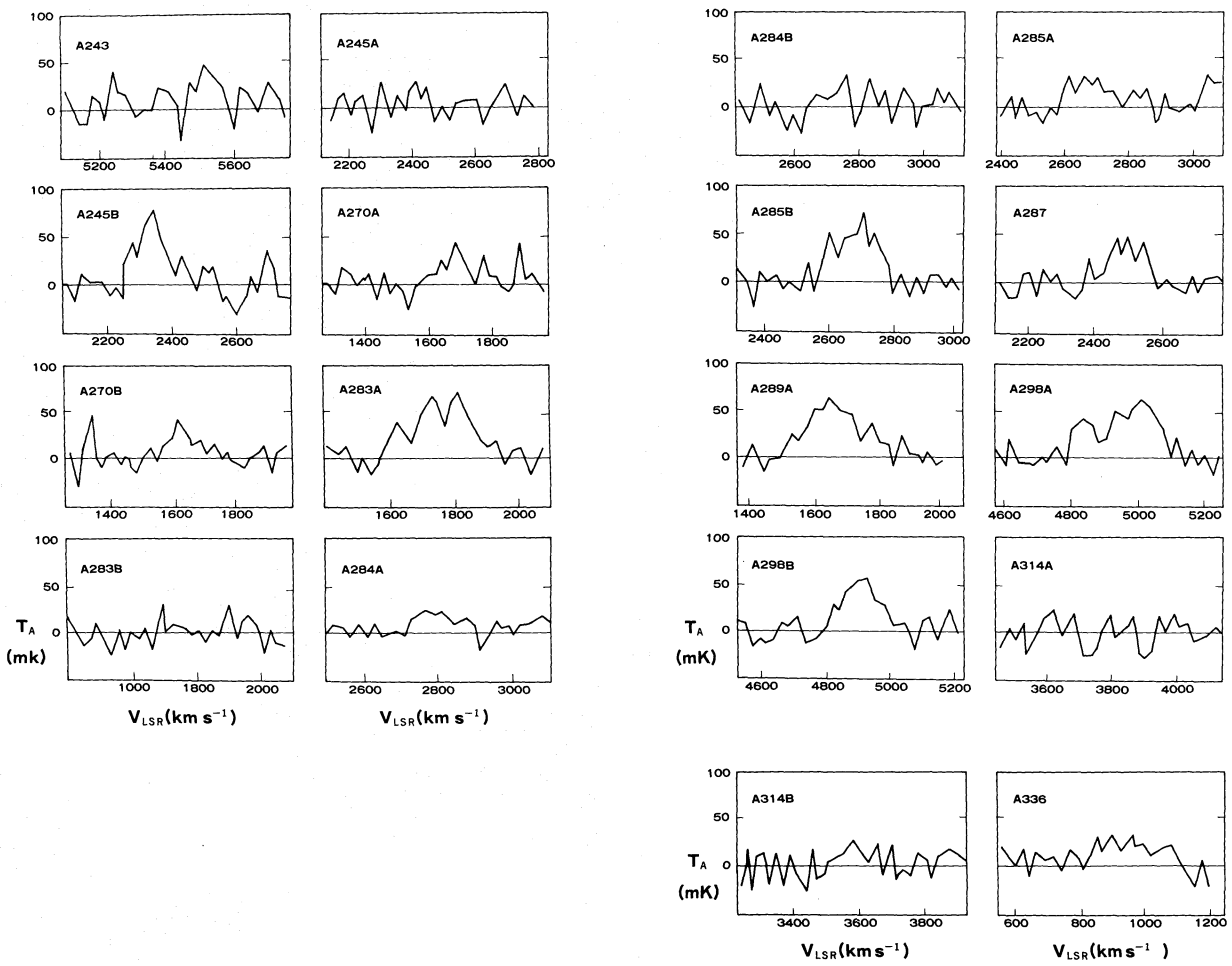

Fig. 1. (Continued)

Column 3: Distance, which is given by V_{GC}/H_0 for a Hubble constant of $H_0 = 75$ km s^{-1} Mpc^{-1}, where V_{GC} is the galacto-centric velocity of the galaxy. For pairs of galaxies, the mean velocity of the two galaxies is used.

Column 4: Beam diameter as projected on the galaxy in kpc. In most cases, since the beam diameter at the galaxy distance is several kpc, the luminosity gives roughly the integrated value. However, for a few galaxies (A135A, A214, A217, A336), the beam covers only the inner 1 kpc. We observed only the upper limits to the antenna temperature for the former three, which were not used in our statistics or correlation analyses. Although data for A336 were used, they were taken so as to give a lower limit for the small covered area on the galaxy.

Column 5: CO luminosity within the central 15″ area as covered by the 45-m telescope beam, where the beam area was calculated by assuming a Gaussian function. The molecular hydrogen mass could be roughly estimated by $M_{H_2}(M_\odot) \sim 6.4 \times L_{CO}$ (K km s^{-1} pc^2) for a nominal conversion relation (Young and Scoville 1982).

Column 6: FIR luminosity as estimated from fluxes taken from the IRAS catalogue of galaxies (Lonsdale et al. 1985), which we interpret as giving the *star-formation rate* (SFR). The FIR luminosity is an integrated value for the entire galaxy, as observed with the IRAS resolution (a few arcmin). Furthermore, in most cases, the pairs of interacting galaxies are observed simultaneously, and the luminosity gives an integrated value for the two galaxies. Therefore, when we compared such IRAS data with other data, for example the CO luminosity, we took the total CO luminosity of the two galaxies.

Column 7: Hα luminosities, taken from Dahari (1985) who used the same Hubble constant used here. Those with asterisks were estimated from the fluxes given by Keel et al. (1985). Note that the Hα observations were made through diaphrams of about 6″ (Dahari 1985) and 5″ (Keel et al. 1985), so that the luminosity is for the more central regions.

Table 1. Observed Arp galaxies.†

(1)* Arp No.	(2) NGC No.	(3) RA_{1950} (h m s)	(4) Dec_{1950} (° ′ ″)	(5) V_{LSR} (km s^{-1})	(6) Peak T_A^* (mK)	(7) σ_V (km s^{-1})	(8) I_{CO} (K km s^{-1})
A86A	N7752	23 44 27.1	29 10 52.0	5038	...	...	...
A86B	N7753	23 44 33.2	29 12 22.0	5160	50	280	7.3
A89A	N2648	08 39 53.3	14 27 58.0	1950	40	260	4.9
A90A	N5929	15 24 18.3	41 50 43.0	2561	∼100	∼170	∼8.5
A90B	N5930	15 24 20.5	41 51 05.0	2498	∼50	250	∼9.4
A91A	N5953	15 32 13.2	15 21 40.0	1950	30	240	7.2
A91B	N5954	15 32 15.7	15 22 10.0	1950	50	190	4.3
A94A	N3226	10 20 43.5	20 09 07.0	1370	∼50	180	∼8
A94B	N3227	10 20 47.6	20 07 00.0	1150	35	300	7.5
A99	N7549	23 12 47.7	18 46 10.0	4689	<20	...	<1
A104A	N5216	13 30 24.6	62 57 27	2949	45	230	9.0
A104B	N5218	13 30 27.8	63 01 27	2792	...	...	...
A112B	N7806	23 58 56.4	31 09 51.0	4801	40	240	6.0
A135A	N1023	02 37 14.9	38 50 52.7	680	<10	...	<1
A140A	N274	00 48 30.0	−07 19 42.0	1750	45	290	7.3
A140B	N275	00 48 32.7	−07 20 00.0	1743	60	270	6.9
A155	N3656	11 20 50.5	54 07 08	2828	<10	...	<1
A160	N4194	12 11 41.7	54 48 21	2550	50	270	6.9
A176A	N7933A	13 01 19.2	−11 13 48.0	3238	<30	...	<3
A176B	N7933B	...	...	...	...	...	...
A178A	N5613	14 22 00	35 07	3100	...	...	...
A178B	N5614	14 22 01.7	35 05 00.0	3891	65	270	8.7
A202	N2719	08 57 07.4	35 55 28.0	3160	50	220	7.7
A205A	UGC6016				<20	...	<1
A205B	N3448	10 51 38.6	54 34 20.0	1340	40	160	3.6
A209	N6052a,B	16 03 01.2	20 40 43	4710	100	250	12.5
A212	N7625	23 18 00.6	16 57 15.0	1620	55	300	12.0
A214	N3718	11 29 50.7	53 20 33	994	<30	...	<3
A215	N2782	09 10 54	40 19 18	2551	<40	...	<0.4
A217	N3310	10 35 40.3	53 45 45.0	1000	75	240	9.0

Table 1. (Continued)

(1)* Arp No.	(2) NGC No.	(3) RA_{1950} (h m s)	(4) Dec_{1950} (° ′ ″)	(5) V_{LSR} (km s^{-1})	(6) Peak T_A^* (mK)	(7) σ_V (km s^{-1})	(8) I_{CO} (K km s^{-1})
A227A	N470	01 17 31.7	03 09 17.0	2343	63	250	8.7
A227B	N474	01 17 10.5	03 08 53.0	2375	30	200	3.6
A239A	N5278A	13 35 47.2	55 55 19.0	7546	<20	...	<2
A239B	N5278B	13 39 51.8	55 55 29.0	7598	55	240	8.4
A240A	N5257	13 37 19.7	01 05 40.0	6881	<20	...	<2
A240B	N5258	13 37 24.7	01 05 10	6643	~70	~150	~10
A243	N2623	08 35 25.3	25 55 35.0	5534	~40	~220	~5
A245A	N2992	09 43 18	−14 05 42	2200	<15	...	<1.5
A245B	N2993	09 43 24.2	−14 08 13	2419	72	300	10.5
A270A	N3395	10 47 02.3	33 14 45.0	1620	40	220	3.8
A270B	N3396	10 47 09.0	33 15 16.0	1620	30	250	3.7
A283A	N2798	09 14 09.5	42 12 37.0	1740	60	380	11.1
A283B	N2799	09 14 18.1	42 12 15.0	1740	<10	...	<1
A284A	N7714	23 33 41.2	01 52 42.0	2800	20	180	2.7
A284B	N7715	23 33 48.5	01 52 48.0	2770	<20	...	<2
A285A	N2854	09 20 39.8	49 25 09.5	2741	25	300	5.7
A285B	N2856	09 20 53.0	49 27 54.0	2680	70	260	8.8
A287A	...	08 59 41.9	26 07 58	2450	40	230	5.7
A289	N3981	11 53 34.0	−19 37 0.0	1723	60	400	11.0
A298A	N7469	23 00 44	08 36 18	4889	60	350	11.1
A298B	...	23 00 46.6	08 37 29.2	4875	55	270	7.6
A314A	...	22 55 27.2	−04 02 15.5	3792	<10	...	<1
A314B	...	22 55 32.4	−04 03 23.6	3581	20	230	2.8
A336	N2685	08 51 41.2	58 55 30.0	880	25	350	7.0

† See the text for legends to individual columns.

* Data for the following galaxies were taken from the literature as shown below: A94A,B, A245A (Taniguchi et al. 1990b); A160, A284 (Taniguchi et al. 1990a); A209 (Sofue et al. 1990); A212 (Yasuda et al. 1992); A336 (Taniguchi et al. 1990c).

Column 8: H I mass, estimated by $M_{H\ I}(M_\odot) = 2.3 \times 10^5 D^2(\mathrm{Mpc}) I_{HI}$ (Jy km s^{-1}), where the H I intensities were taken from Huchtmeier and Richter (1989).

Column 9: Interaction class (IAC), which was evaluated by inspecting objects in the Arp's catalogue (Arp 1966) in accordance with the definition introduced by Dahari (1985). Galaxies with 0/6 are single peculiars, possiblly superimposed by merged components.

Column 10: Star-formation efficiency (SFE), as defined by the ratio of L_{FIR} to L_{CO} in the same units as in columns 6 and 5. This indicates the *star-formation efficiency* from the molecular hydrogen gas.

Column 11: SFE as defined by $L_{H\alpha}$ /L_{CO} in the same units as in columns 7 and 5. This indicates a more nuclear star-formation efficiency.

Column 12: SFE as defined by L_{FIR}/ $M_{H\ I}$ in the same units as in columns 6 and 8. This indicates the efficiency of star formation compared to the total H I mass.

Table 2. CO, FIR, and Hα luminosities, H I masses, their ratios and IAC for Arp galaxies.†

(1) Arp No.	(2) Type	(3) Dist. (Mpc)	(4) Beam (kpc)	(5) L_{CO} (10^7 K km s^{-1} pc^2)	(6) I_{FIR} ($10^8 L_\odot$)	(7) $L_{H\alpha}$ ($10^6 L_\odot$)	(8) M_{HI} ($10^9 M_\odot$)	(9) IAC	(10) SFE FIR/CO	(11) SFE Hα/CO	(12) SFE FIR/HI
A86A	Im	71	5.2	...	500		9.2	2	...	...	...
A86B	Sc			22	〃	77	15.1	2	23	3.5	47
A89A	Sa	25	1.8	1.84	7.4		0.38	1	4	...	19
A90A		36	2.6	~6.6	300	5		4	22	0.8	250
A90B	Sa			~7.3	〃	7	1.2	4	〃	1	〃
A91A	S0	27	2.0	3.2	190	6	1.2	5	37	1.9	160
A91B	Sc			1.9	〃	4		5	〃	2	〃
A94A	E2	16	1.2	1.2	60		0.4	5	...	...	...
A94B	Sa			1.2	〃	31	1.2	5	25	25	50
A99B	SBcd	64	4.6	<3	165		3.2	1	...	...	50
A104A	Ep	40	2.9	8.6	92	1.6		2	11	0.2	80
A104B	SBb	...	...	...	〃	1.0	1.2	2	...	...	〃
A112B	Sb,c	66	4.8	16	...	0.8*	1.3	3	...	0.11	...
A135A	SB0	10.5	0.76	<0.1	...		0.8	2	...	...	...
A140A	S0p	24	1.8	2.5	70		2.6	5	14	...	19
A140B	SBcd			2.4	〃		3.6	5		...	
A155	S0a(S)	42	3.1	<1.0	90		1.0	0/6	...	...	90
A160	IBm	35	2.6	4.9	670	68	1.2	6	137	14	600
A176A	S0p	42	3.1	<3	...	...	...	2	...	...	...
A176B	...	...	...	...	...	...	...	2	...	...	...
A178A	...	53	3.9	...	101			2	...	...	...
A178B	Sab			14.6	〃	4	1.5	2	6.9	0.27	67
A202A	Im	42	3.1	8.1	60		6.5	3	7.4	...	9
A205A	SBd	19	1.4	<0.3	50		4.4	2	...	...	...
A205B	I0,S0,a			0.8	〃		4.5	2	6.2	...	11
A209	Im	64	4.7	30.7	665	28	8.6	6	22	0.91	80
A212	Sa0p(S)	24	1.8	4.1	130	6.2	2.4	0/6	32	1.5	60
A214	SBa(S)	14	1.0	<0.3	2		4.3	0/6	...	...	0.5
A215	Sa(S)	34	2.5	<3	250		3.8	0/6	...	...	70
A217	Sbc(S)	14	1.0	1.1	150	6.7	2.8	0/6	136	6.1	55

Table 2. (Continued)

(1) Arp No.	(2) Type	(3) Dist. (Mpc)	(4) Beam (kpc)	(5) L_{CO} (10^7 K km s^{-1} pc^2)	(6) I_{FIR} ($10^8 L_\odot$)	(7) $L_{H\alpha}$ ($10^6 L_\odot$)	(8) M_{HI} ($10^9 M_\odot$)	(9) IAC	(10) SFE FIR/CO	(11) SFE Hα/CO	(12) SFE FIR/HI
A227A	Sb	32	2.3	5.3	170	5*	4.5	2	23	0.9	60
A227B	S0			2.2	〃	0.15*	<0.8	2	〃	0.07	〃
A239A	Sb?	103	7.5	<20	370	9	4.1	5	...	...	90
A239B	Sb			53	〃			5	7.0	...	...
A240A	Sb?	89	6.5	<10	2020	5	12	4	...	...	180
A240B	Sb			~47	〃	6	9.8	4	43	0.13	205
A243	Pec	73	5.3	16	2600	4.7	1.7	6	163	0.29	1500
A245A	Sa	30	2.5	<1	180		5.6	3	...	...	35
A245B	Sab			5.7	220			3	39	...	40
A270A	Scd	21	2.2	1.0	80	0.7	2.1	4	40	0.7	35
A270B	SBm		1.5	1.0	〃	2.1	2.2	4	〃	2.1	〃
A283A	SBa	23	1.7	2.5	280	1.2	0.39	5	80	0.34	220
A283B	SBm			<0.3	〃	0.08	1.2	5	〃	...	〃
A284A	SBb	39	2.8	2.5	400	57	7.4	4	160	23	50
A284B	IBm			<2	〃	0.3	3.9	4	...	...	
A285A	SBc?	36	2.6	4.7	190		3.1	2	16.5	...	60
A285B	Sb			6.8	〃			2	〃	...	〃
A287A		32	2.3	3.5	40			3	11	...	...
A289	Sbc	21	1.5	2.9	90	1.1	5.7	2	31	0.38	16
A298A	SBa	67	4.9	30.0	3070		2.8	2	61	...	1100
A298B				20.4	〃			2	〃	...	〃
A314A		50	3.6	<3	...			1	...	...	...
A314B				4.2	...			1	...	...	...
A336	S0(S)	12	0.87	0.6	1		1.1	0/6			

† See the text for legends to individual columns.

3.2. Correlations among Luminosities

In order to visualize the derived parameters, we plotted various quantities (figures 2 to 5). We did not use the upper-limit value data, since they are dependent on the observation conditions.

FIR vs CO: Figure 2 shows plots of L_{FIR} versus L_{CO} for the detected Arp galaxies. As noted above, if a pair of galaxies was observed within the IRAS beam, we added the two CO luminosities to produce a single point in the diagram. Therefore, most of the points in the diagram are for the integrated values of pairs. The figure indicates that almost all of the observed Arp galaxies lie far above the line fitted for normal galaxies, and that the plot resembles that for IR luminous and starburst galaxies (Sanders et al. 1986; Young et al. 1986). This fact shows either that the efficiency of massive-star formation from molecular gas in the observed galaxies is higher

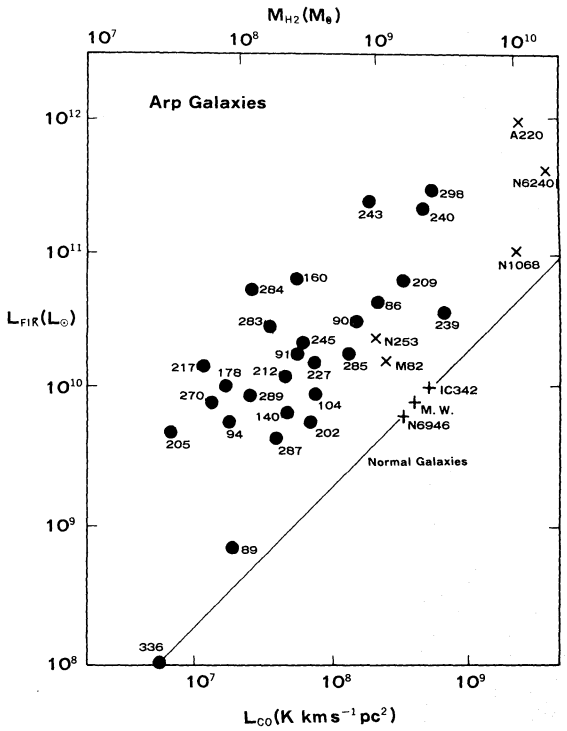

Fig. 2. Plot of $L_{\rm FIR}$ versus $L_{\rm CO}$ for the detected Arp galaxies. Note that $L_{\rm CO}$ is for the central 15″ area as covered by the 45-m telescope beam, while $L_{\rm FIR}$ is an integrated value for the whole galaxy as observed with the IRAS (Lonsdale et al. 1985). Dark circles indicate data from the present observations, and crosses (× for starburst galaxies; + for normal galaxies) are taken from the literature (Sanders et al. 1986; Young et al. 1986).

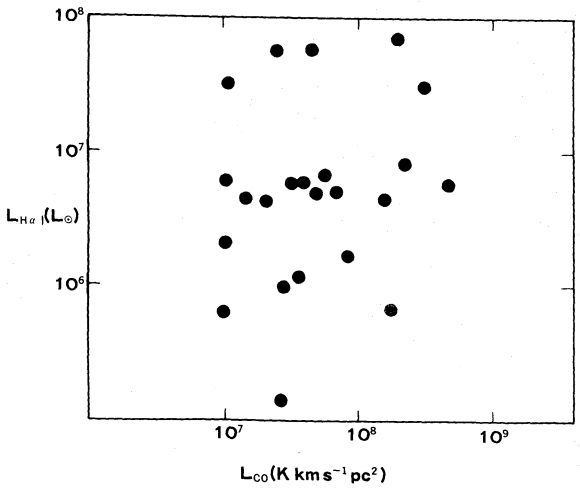

Fig. 3. Hα luminosity $L_{\rm H\alpha}$ versus CO luminosity $L_{\rm CO}$.

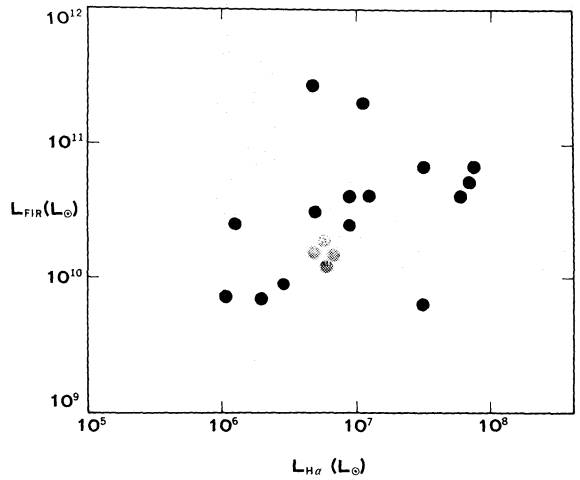

Fig. 4. FIR luminosity $L_{\rm FIR}$ versus Hα luminosity $L_{\rm H\alpha}$.

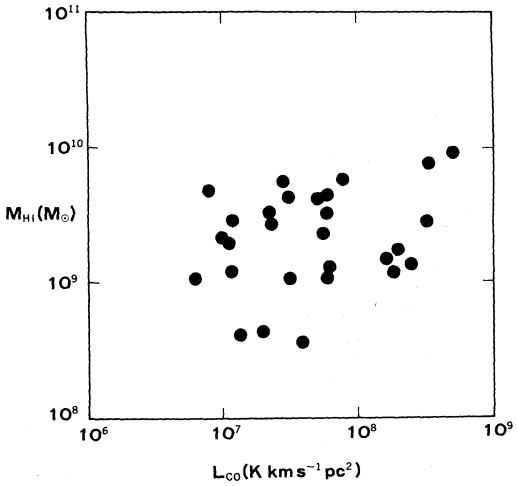

Fig. 5. H I mass $M_{\rm H\ I}$ versus CO luminosity $L_{\rm CO}$.

than that for normal galaxies, or that much of the FIR emission comes from outside the telescope beam of 15″. The former indicates that the galaxy-galaxy interaction enhances star formation; the latter suggests that active star formation is in progress even in galactic disks a few kpc away from the nuclei.

Hα vs CO: Figure 3 plots Hα luminosity versus CO luminosity. It is hard to find any correlation. Since Hα data are taken with 5″ to 6″ diaphragms, we plot here individual galaxies. The fact that the FIR to CO correlation in figure 2 is much better than the Hα to CO correlation may indicate that the star formation is enhanced in a wider (a few to several kpc) region than the central few hundred pc region.

FIR vs Hα: Figure 4 shows plots of the FIR luminosity versus the Hα luminosity. Again, no significant correlation can be recognized. The weak correlation between Hα and FIR emission may be due to the significant difference between the beam areas of observations. FIR data come from IRAS observations, where the beam is a few arcmin (Lonsdale et al. 1985); the Hα observations were made by a diaphram of 5″ to 6″ (cenetral few hundred pc) or

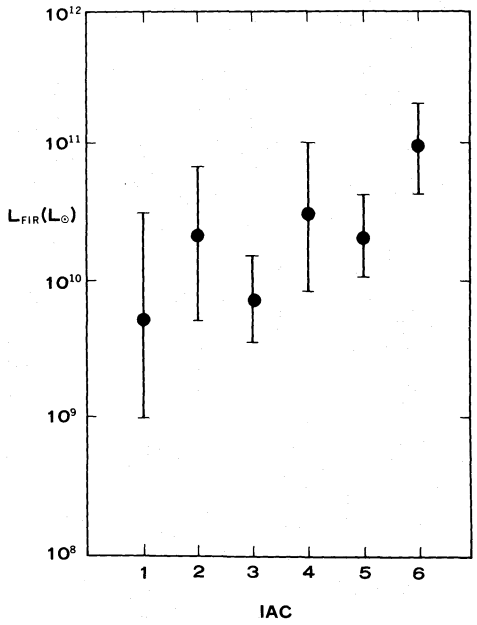

Fig. 6. FIR luminosity plotted against the interaction class IAC.

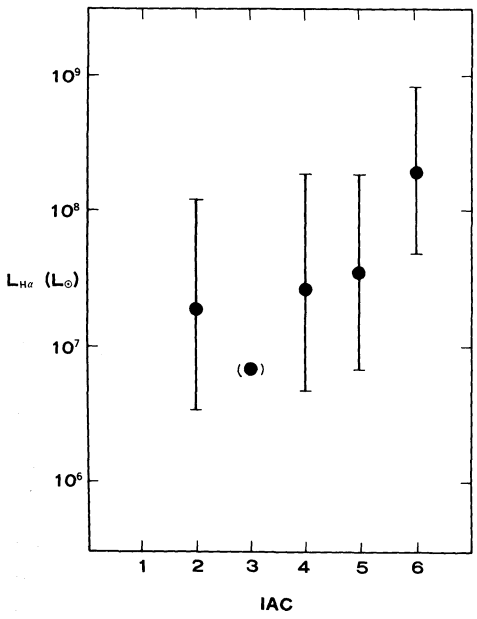

Fig. 7. Hα luminosity versus IAC.

more, indicating nuclear activity (Dahari 1985; Keel et al. 1985).

H I vs CO: Figure 5 shows plots of the H I mass against the CO luminosity, which is approximately proportional to the molecular hydrogen mass. Almost no correlation has been found between H I and CO. The H I mass is approximately concentrated in the range between 10^9 and $10^{10} M_\odot$, while the molecular hydrogen mass is widely distributed. Note that the H I mass is for the entire galaxy, due to the larger beam of observations, while the H_2 mass is for the central few kpc.

3.3. *Correlations of Luminosities with Interaction Class*

In order to clarify the relation between star formation and galaxy interaction, we investigated correlations of the observed values with the interaction class (IAC), as introduced by Dahari (1985), where IAC=1: double galaxies without significant deformation; IAC=3: interacting galaxies with deformation; IAC=5: strong interaction; IAC=6: almost superposed configuration, possibly merging.

FIR vs IAC: Figure 6 shows plots of $L_{\rm FIR}$ against IAC (interaction class). Each point indicates an average of several galaxies having the same IAC value. The bar indicates the dispersion among the vlaues for the averaged galaxies. We found that the *star-formation rate* is generally enhanced by the interaction, particularly for very strongly interacting galaxies with IAC=6. Note that, as is shown in section 3.4 below, this enhancment of SFR is not due to a larger amount of molecular gas, but to an enhancment of star-formation efficiency.

Hα vs IAC: Figure 7 shows plots of $L_{\rm H\alpha}$ against IAC. The data are more scattered than in figure 6, and show a similar trend to that in figure 6. The point indicated by parentheses includes only one data point; no dispersion is given.

CO vs IAC: Figure 8 shows plots of $L_{\rm CO}$ versus IAC. There appears to be no correlation in this diagram, which indicates that the molecular gas concentration toward the central few kpc is not efficiently enhanced in these interacting galaxies.

H I vs IAC: Figure 9 shows plots of $M_{\rm H\ I}$ versus IAC. No correlation can be found, and this is not surprising, due to the widely spread nature of the H I gas content in the galaxies.

3.4. *Correlations of Star-Formation Efficiencies with Interaction Class*

In so far as the correlation diagrams shown in figures 6 to 9 are concerned, no clear correlation can be found with the interaction class, except for the signature of an enhancement of the star-formation rate, as in figure 6. Nevertheless, we have observed a significant tendency for the FIR luminosities to exceed those for normal galaxies, as in figure 2. In this context we next examined the correlation of IAC with star formation efficiencies, as derived from the ratio of $L_{\rm FIR}/L_{\rm CO}$, $L_{\rm H\alpha}/L_{\rm CO}$, or $L_{\rm FIR}/M_{\rm H\ I}$. Figures 10 to 12 show the results.

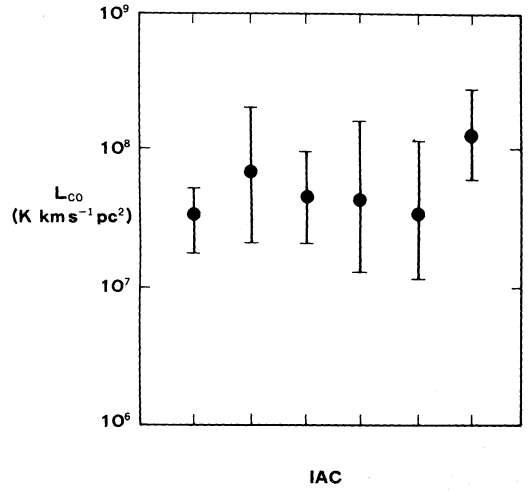

Fig. 8. CO luminosity (molecular hydrogen mass) against IAC.

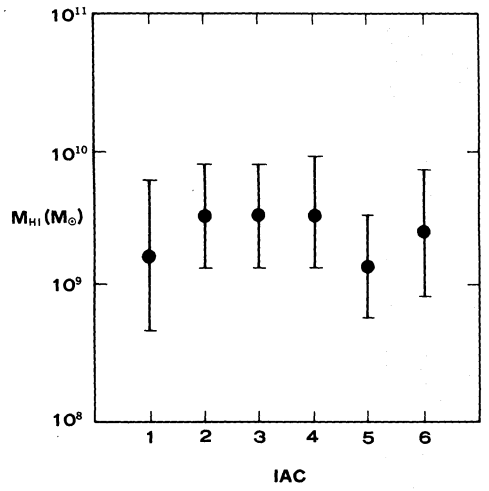

Fig. 9. H I mass against the IAC.

SFE(FIR/CO) vs IAC: Figure 10 shows plots of the star-formation efficienty, as defined by SFE (FIR/CO) = $L_{\rm FIR}/L_{\rm CO}$, agaist IAC. Here, we can see a better correlation than that for star-formation rate as inferred from $L_{\rm FIR}$: the efficiency of star formation from molecular hydrogen gas is enhanced by the galaxy-galaxy interaction. We may also say that the correlation observed in figure 6 for $L_{\rm FIR}$ is due to an enhanced efficiency per molecular gas, and not due to any increase in the net fuel (molecular gas) available for star formation.

SFE(Hα/CO) vs IAC: Figure 11 shows plots of SFE (Hα/CO)= $L_{\rm H\alpha}$ /$L_{\rm CO}$ against the interaction class. A similar, but weaker, correaltion to figure 10 is observed. We also note that the scatter in this diagram is much larger than in figure 10. Such a large scatter may also occur for a large obscuration of the Hα emission toward the central region due to the circum-nuclear molecular gas.

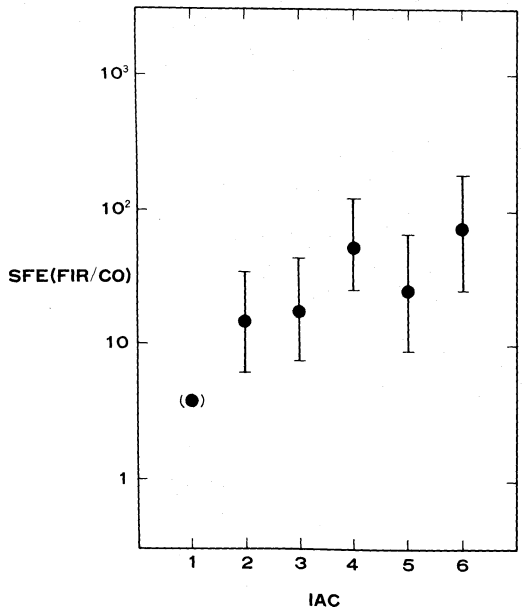

Fig. 10. SFE (FIR/CO)=$L_{\rm FIR}/L_{\rm CO}$, plotted against IAC.

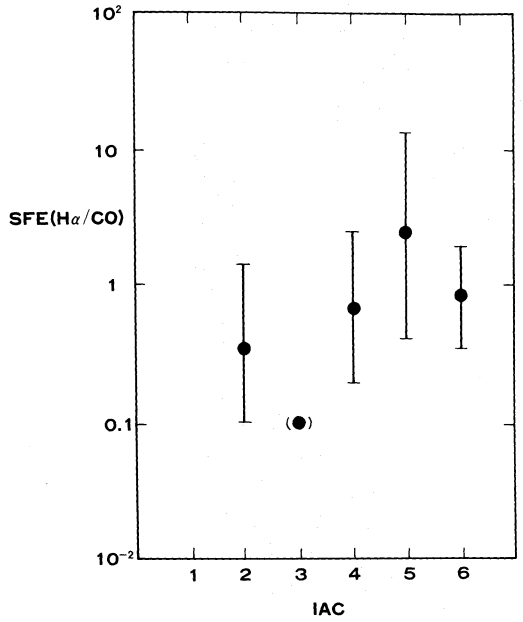

Fig. 11. SFE (Hα/CO)= $L_{\rm H\alpha}$ /$L_{\rm CO}$, plotted against IAC.

SFE(FIR/H I) vs IAC: Figure 12 shows plots of SFE (FIR/H I)=$L_{\rm FIR}$/ $M_{\rm H\ I}$ versus IAC. A similar correlation to that in figure 10 is found, with a particular increase at IAC$\sim$ 6.

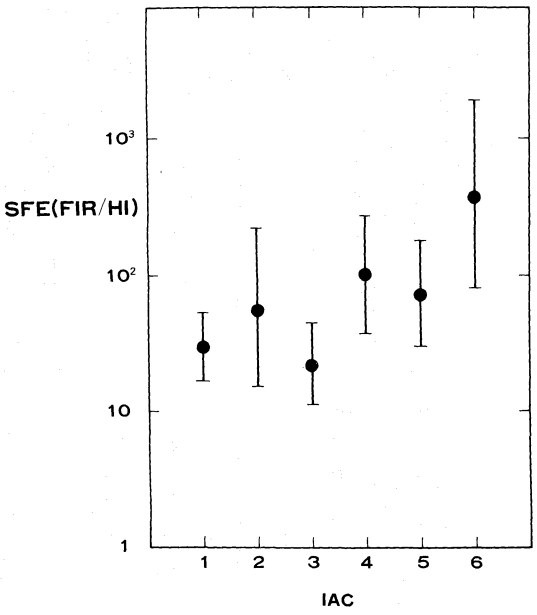

Fig. 12. SFE (FIR/H I)=$L_{\rm FIR}/\ M_{\rm H\ I}$, plotted against IAC.

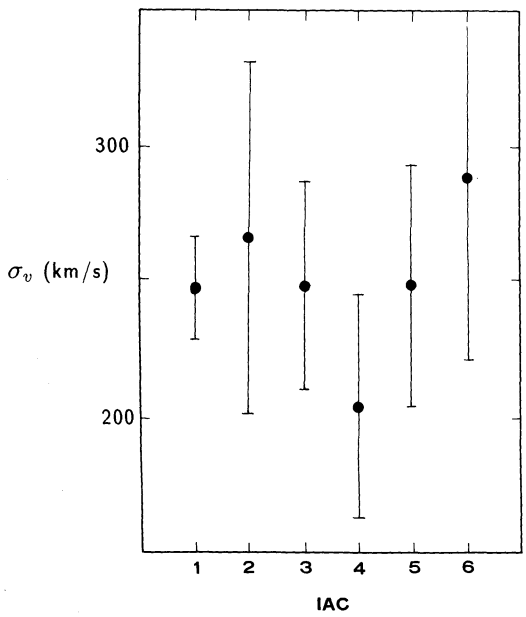

Fig. 13. Velocity dispersion of CO profiles, σ_v, plotted against IAC.

From these plots we can reach the following important conclusion. The molecular gas concentration in the central few kpc is not significantly affected by the interaction (figure 8). However, the efficiency of star formation from molecular gas is strongly influenced by the tidal interaction (figure 10). Namely, although *the gas concentration toward the central few kpc is not necessarily enhanced by the interaction, the efficiency of star formation increases via the tidal interaction.* We may also state that star formation close to the galactic nuclei, as indicated from the SFE (Hα/CO), is also enhanced by the interaction (figure 11).

3.5. *Correlations with Velocity Dispersion*

Since the galaxies studied here are mostly interacting galaxies, their intermal kinematical condition would be affected by the interaction. The velocity dispersion for the CO gas as determined from the velocity profiles given in figure 1, would reflect some kind of kinematical structure, such as a tidal disturbance.

Velocity dispersion vs IAC: Figure 13 shows plot of the CO velocity dispersion (σ_v) against the IAC. There seems to be no clear correlation, although data for high IAC galaxies are more scattered than those for weakly interacting galaxies. This would be because the velocity dispersion is more correlated to the inner galactic rotation of the order of a few hundred km s^{-1}. The innermost region is not directly disturbed by a tidal interaction, at least by an amount comparable to the rotation velocity. Nevertheless, the internal kinematics would be affected by the tidal interaction by such an accretion process, such as bar-induced shocks, while velocities caused by these motions would be of the order of a few tens of km s^{-1} (e.g., Noguchi 1988), small compared to the dispersion produced by inner-disk rotation.

On the other hand, gas in the outermost regions would be more directly disturbed by the tidal interaction. In this context, it would be interesting to plot the H I velocity dispersions against IAC, though this is beyond the scope of this paper.

SFE vs velocity dispersion: Finally, we plot the star-formation efficiency [SFE (FIR/CO)] against the velocity dispersion given in figure 14. Again, we find no significant correlation, which is a reasonable consequence of the absence of a correlation between the velocity dispersion and IAC, as shown in figure 13.

On the other hand, we know that the SFE increases with IAC (figure 10): this correlation should be related to some change in the kinematical conditions in molecular clouds, such as accumulation and compression in the disk. Although the internal kinematics should be affected by a tidal interaction through such an accretion process as bar-induced shocks, the velocities caused by these motions would be of the order of a few tens of km s^{-1} (e.g., Noguchi 1988), small compared to the dispersion produced by the total disk rotation.

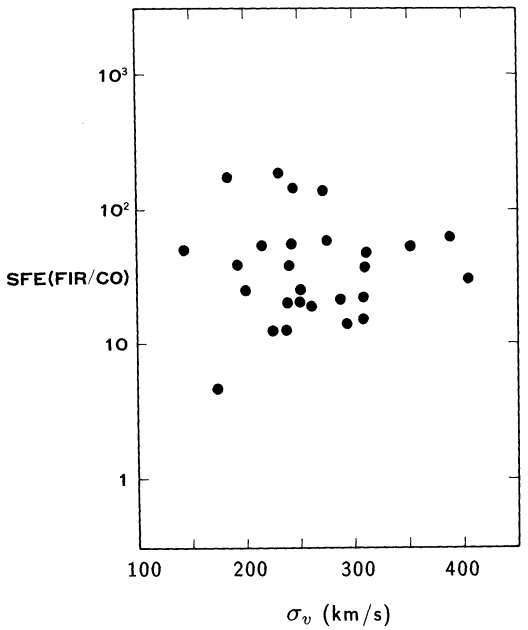

Fig. 14. SFE (FIR/CO)=$L_{\rm FIR}/L_{\rm CO}$, plotted against CO velocity disperion.

4. Conclusion

We performed CO ($J = 1-0$) line obserations of fifty-four Arp's interacting galaxies of various types and interaction classes. Plots of $L_{\rm FIR}$ versus $L_{\rm CO}$, as in figure 2, indicate that the far-infrared luminosities, as normalized by the CO luminosities, are much higher for interacting galaxies than for normal galaxies, and resemble those observed for starburst galaxies.

Quantities such as $L_{\rm CO}$ and $M_{\rm H\ I}$ seem to show almost no significant correlation with the interaction class IAC, as can be seen from the plots against IAC in figures 8 and 9. We may therefore conclude that the amount of molecular gas in the central few kpc is not significantly affected by the interaction (figure 8). However, the plots of the star-formation rate (SFR) and efficiencies (SFE) against IAC clearly indicate that they are significantly enhanced by some interaction (figures 6 and 10). We stress that the increase in SFE is the cause for the increase in the star-formation rate (SFR), as found in figure 6 despite the absence of any correlation between the gaseous content and IAC (figures 8 and 9). Namely, *the galaxy-galaxy interaction does not necessarily gather up gas, but it enhances the efficiency of star formation* from a unit mass of molecular gas, which results in an apparent increase in the total rate of star formation.

This work was financially supported by the Ministry of Education, Science and Culture under Grant No. 01420001 and 01302009 (Y. Sofue). We thank T. Sayano of the Kiso Observatory for measuring the center positions of program galaxies. We thank T. Handa, N. Yasuda, K. Fujisawa, S. Uemura, S. Hoshi, T. Kikumoto, and S. Takagi for helping us in the observations and data reduction. We are also indebted to Dr. K. Kawara for a critical reading of the manuscript as the referee, and for the valuable comments.

References

Arp, H. 1966, in *Atlas of Peculiar Galaxies* (California Institute of Technology, California), p. 48.
Dahari, O. 1985, *Astrophys. J. Suppl.*, **57**, 643.
Huchtmeier, W. K., and Richter, O.-G. 1989, in *A General Catalog of H I Observations of Galaxies* (Springer-Verlag, Heidelberg), Table 1.
Huntley, J. M., Sanders, R. H., and Roberts, W. W., Jr. 1978, *Astrophys. J.*, **221**, 521.
Keel, W. C., Kennicutt, R. C., Jr., Hummel, E., and van der Hulst, J. M. 1985, *Astron. J.*, **90**, 708.
Lonsdale, C. J., Helou, G., Good, J. C., and Rice, W. L. 1985, in *Catalogued Galaxies and Quasars Observed in the IRAS Survey* (US Government Printing Office, Washington, D.C.).
Noguchi, M. 1988, *Astron. Astrophys.*, **203**, 259.
Rieke, G. H., Lebofsky, M. J., Thompson, R. I., Low, F. J., and Tokunaga, A. T. 1980, *Astrophys. J.*, **238**, 24.
Sanders, D. B., Scoville, N. A., Young, J. S., Soifer, B. T., Schloerb, F. P., Rice, W. L., and Danielson, G. E., 1986, *Astrophys. J. Letters*, **305**, L45.
Sofue, Y. 1987 in *Proc. NATO Advanced Institute* on *Galactic and Extragalactic Star Formation*, ed. R. Pudritz (D. Reidel Publishing Company, Dordrecht), p. 409.
Sofue, Y., Taniguchi, Y., Wakamatsu, K., Nakai, N., Handa, T., Fujisawa, K., and Yasuda, N. 1990, *Publ. Astron. Soc. Japan*, **42**, L45.
Solomon, P. M., and Sage, L. J. 1988, *Astrophys. J.*, **334**, 613.
Sørensen, S.-A., Matsuda, T., and Fujimoto, M. 1976, *Astrophys. Space Sci.*, **43**, 491.
Taniguchi, Y., Kameya, O., Nakai, N., and Kawara, K. 1990a, *Astrophys. J.*, **358**, 132.
Taniguchi, Y., Kameya, O., and Nakai, N. 1990b, in *The Interstellar Medium in External Galaxies*, ed. D. J. Hollenbach and H. A. Thronson, Jr. (NASA Conf. Publ. No. 3084), p. 56.
Taniguchi, Y., Sofue, Y., Wakamatsu, K., and Nakai, N. 1990c, *Astron. J.*, **100**, 1086.
Telesco, C. M. 1988, *Ann. Rev. Astron. Astrophys.*, **26**, 343.
Yasuda, N., Fujisawa, K., Sofue, Y., Taniguchi, Y., Nakai, N., and Wakamatsu, K. 1992, *Publ. Astron. Soc. Japan*, **44**, 1.
Young, J. S., Kenney, J. D., Tacconi, L., Claussen, M. J., Huang, Y.-L., Tacconi-Garman, L., Xie, S., and Schloerb, F. P. 1989a, *Astrophys. J. Letters*, **311**, L21.
Young, J. S., and Scoville, N. Z. 1982, *Astrophys. J.*, **258**, 467.
Young, J. S., Xie, S., Kenney, J. D. P., and Rice, W. L. 1989b, *Astrophys. J. Suppl.*, **70**, 699.
Young J. S., Schloerb, F. P., Kenney, J. D., and Lord, S. D. 1986, *Astrophys. J.*, **304**, 443.